Hamous, H.; Khenifi, A.; Orts Maiques, FJ.; Bonastre Cano, JA.; Cases, F. (2021). Carbon textiles electrodes modified with RGO and Pt nanoparticles used for electrochemical treatment of azo dye. Journal of Electroanalytical Chemistry. 887:1-10. https://doi.org/10.1016/j.jelechem.2021.115154

Carbon textiles electrodes modified with RGO and Pt nanoparticles used for electrochemical treatment of azo dye

Hanene Hamous[a], Aicha Khenifi[a], Francisco Orts[b], José Bonastre[b] and Francisco Cases[b]*

[a] Physical and Chemical Laboratory of Materials, Catalysis and Environment (LPCMCE) Faculty of Chemistry University of Sciences and Technology of Oran (USTO M-B), BP 1505 Oran, Algeria

[b] Departamento de Ingeniería Textil y Papelera, EPS de Alcoy, Universitat Politècnica de València, Plaza Ferrándiz y Carbonell s/n, 03801 Alcoy, Spain

*Corresponding author: F. Cases (fjcases@txp.upv.es)

ABSTRACT

The efficiency of Orange G (OG) azo dye degradation using an electrochemical method under potentiostatic conditions has been comparatively studied in two electrolytic cells (divided and undivided cells) in the presence or absence of chloride ions with Pt-modified textile electrodes. The morphology of the carbon-based electrodes with nanoparticles of platinum electrochemically dispersed on their surface was analyzed using field emission scanning electron microscopy (FESEM) and EDX analysis. The FESEM analyses confirmed that the textile surface was coated by Pt nanoparticles. According to the experimental results obtained, when the same solutions are comparatively treated with the two cells, the undivided cell always gives a quicker decolorization than the divided cell – and the decrease in total organic carbon (TOC), chemical oxygen demand (COD), and total nitrogen (TN) confirms this result. The degree of OG removal was monitored by spectroscopic methods and high-performance liquid chromatography (HPLC). The results indicate that that full best dye removal is obtained at a loaded charge of around 0.17 Ah L^{-1} which is associated with an electrical energy per order (EEO) of 0.189 kWh m^{-3} $order^{-1}$. Based on the results obtained, the electrochemical process with TC-RGO-Pt electrodes could be useful as a pretreatment technique or treatment for decolorizing wastewaters containing dyes.

Keywords: Carbon textiles electrodes; reduced graphene oxide; platinum nanoparticles; Orange G; electrochemical treatment

1 Introduction

Direct discharges of colored effluents into the aquatic environment have become an environmental issue in recent years [1]. The problem arises from the quantity, chemical composition, and non-biodegradable nature of some of the dyes used in industry [2] and whose derivatives can be toxic, carcinogenic, teratogenic, or mutagenic [3]. Their resistance to oxidation [4] and chemical stability gives them a sustained persistence in the environment and makes them highly toxic organic pollutants. Moreover, these pollutants are difficult to remove using conventional wastewater treatment technologies [5]. In order to limit the entry of these refractory contaminants into the environment, effective and environmentally friendly treatment strategies have been developed. Among these strategies is the application of electrochemical processes. These techniques can provide a solution for the treatment of wastewater, whether by the separation of toxic or recoverable species or by conversion on the surface of the electrode through the electronic exchange. These processes are specific because are environmentally friendly and do not generate new toxic waste [6]. Among electrochemical processes, anodic electro-oxidation is the most popular process for the removal of organic pollutants from wastewater [7;8]. However, the efficiency of electrochemical oxidation of dyes in aqueous solutions depends strongly on the nature of the electrode used [9]. Different types of electrodes including active carbon fiber (ACF) [10], Pt [11], Ti / SnO_2 [12] , boron-doped diamond (BDD) [13], Ti / RuO_2 [14], IrO_2 / TaO_2 / RuO_2, [15], RuO_2 [16], PbO_2, [17-19], Ti / IrO_2 / SnO_2 / Sb_2O_5 [3] and Ti / SnO_2-Sb [20] were used in electro-oxidation dye degradation studies. The choice of the electrode in an electrochemical process is crucial because it greatly influences the selectivity and efficiency of the process. An electrode must have the following criteria: (1) high physical and chemical stability, and therefore high corrosion resistance; (2) high electrical conductivity; (3) presence of catalytic activity; and (4) a good relationship between cost and lifespan [21]. It should also be noted that an anode must have a fairly high oxygen evolution potential (high oxygen overvoltage) to produce a relatively high concentration of hydroxyl radicals [22]. Other criteria such as the type of substrate, the method of deposition, as well as the type of dopant are important to emphasize [23]. Textile materials, such as substrates for electrodes, offer many possibilities due to their mechanical properties, such as flexibility, and many possibilities for the design of compact electrochemical reactors with competitive costs. The use of activated carbon textiles (TC) adds interesting properties such as a high specific area and electronic conductivity. At the same time, a carbon fiber surface enables the adsorption of species that can react physically and chemically when the electrode is polarized [24]. Moreover, the special structure of graphene has excellent mechanical properties (Young's modulus and

breaking strength is 1100 GPa and 125 GPa, respectively), excellent electrical properties (electron mobility is 200 000 cm2 /(V•s)) [25], excellent thermodynamic properties (5300 W/(m•k), and large specific surface area (2600 m2 /g)[25]. This revolutionary discovery has rapidly attracted scholars from physical, chemical, and biological fields. Graphene oxide (GO) is well known as a promising precursor of graphene. Due to the presence of these oxygen-containing functional groups, graphene oxide not only has a large theoretical specific surface area (up to 400-1500 m^2 g^{-1})[26], but also offers an efficient use of surface area because both sides of the nanosheet are accessible. Chemical reduction is a common strategy to reduce GO into reduced graphene oxide (RGO). Unfortunately, this method generally uses reducing agents that are toxic or explosive: such as hydrazine [27] and dithionite salts [28]. As a result, continuous efforts have been directed towards finding an eco-friendly reducing method for GO reduction. The electrochemical reduction of GO is an alternative that relies on the removal of oxygen functionalities [29,30]. The use of TC as electrode substate, an electrically conductive material, makes this possible. Moreover, its high specific surface area makes graphene interesting for dispersing Pt nanoparticles to modify the electrode surface; and graphene oxide (RGO) and graphene show improved electrocatalysis performance and stability [31,32].

There is considerable literature published on OG degradation [33-35]. However, until now there was no available literature about electrochemical degradation of OG using textile electrodes with reduced graphene oxide-based electrodes coated with dispersed platinum, these electrodes have been named in this work with the abbreviation TC-RGO-Pt, with the objective of decreasing costs and energy consumption. In this paper, the use of divided and undivided cells was carried out under comparable conditions to test the degradation ability of each electrolytic system. The stability of TC-RG-Pt electrodes in these experimental conditions was evaluated.

2 Experimental

2.1 Reagents and materials

All reagents used were of analytical grade with a purity level > 98%. Monolayer GO powders were supplied by Nanoinnova Technologies SL (Spain). $LiClO_4$, H_2SO_4 and $H_2PtCl_6{\cdot}6H_2O$ were purchased from Merck. Pt wires (0.5 mm diameter, 99.99% purity) were acquired from Engelhard-Clal. FlexzorbTM FM10 activated carbon fabrics electrodes (TC) were kindly donated by Chemviron Carbon. Na_2SO_4 and NaCl (Fluka quality of analysis) were selected as the supporting electrolytes in this work. The solutions were prepared with ultrapure water obtained from a Millipore Milli-Q system (resistivity ≥ 18.2 MΩ cm).

2.2 Pollutant dye

Orange G ($C_{16}H_{10}N_2Na_2O_7S_2$; MW 452,38 g mol^{-1}) is an azo dye obtained from Across Organics. [36]. Fig 1 shows the chemical structure of the dye and the UV-Vis wavelength characteristics associated with its structure.

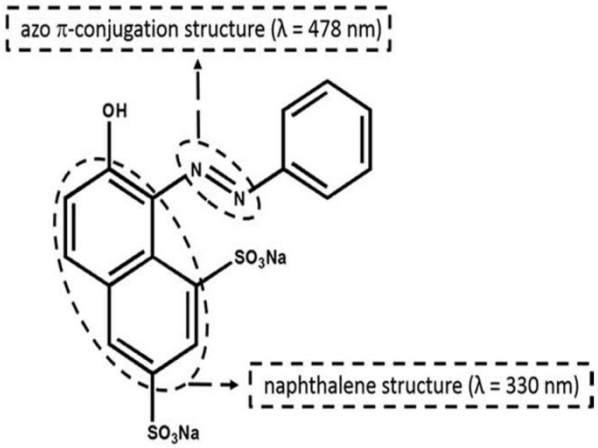

Fig.1. A scheme for the chemical structure of orange G [35]

2.3 Electrode preparation

2.3.1 Manufacture of the electrodes

The TC electrodes are prepared by cutting a 1 cm x 1 cm strip from the carbon fiber fabric which is glued with Circuit Works® conductive epoxy resin by Chemtronics® to a copper wire with a flattened end of 2 mm diameter. A drop of non-conductive epoxy resin seals the electrical contact on the fabric fold. The solder is dried in the oven at 85°C and protected with Teflon tape.

2.3.2 TC/RGO/Pt electrode preparation

The electrochemical synthesis of reduced graphene oxide (RGO) and Pt nanoparticles on the TC surface was performed by the potentiodynamic method of cyclic voltammetry (CV) at room temperature with a potentiostat/galvanostat Autolab PGSTAT30 using a cone-shaped voltammetric cell. All electrochemical manipulations were performed using a reference electrode type Ag/AgCl (3.5 M).The textile electrode (TC) was immersed in an electrodeposition solution A. The latter is prepared by dissolving 3 $g.L^{-1}$ of GO in 0.1 M LiClO4. The electrochemical treatments are carried out in a potential range from -1.6 V to 0.6 V for 20 cycles at a scanning speed of 20 mV s^{-1}, using a Pt wire as a counter electrode (CE).Then, the textile electrode previously electrodeposited by the RGO is immersed a second time in solution B containing 5 mM H_2PtCl_6 and 0.5 M H_2SO_4 . This time a cylindrical stainless-steel mesh 4.5 cm high by 3.5 cm wide is used as a counter electrode, the potential

range used was from +0.4 V to −0.25 V using a scanning speed of 10 mV s^{-1}. Before each experiment, the solutions were deaerated with N_2 for 30 min. During the RGO synthesis, the GO solution was gently stirred with a magnetic stirrer to avoid precipitation of GO. Finally, the sample was air-dried for 24 hr. The presence of an effective and significant amount of Pt was demonstrated by electrochemical and FESEM analyses. The electrodes prepared in this way have been named with the abbreviation TC-RGO-Pt

2.4 Characterization methods

2.4.1 Electrode characterization

The microstructure and morphology of the electrodes were analyzed by field emission scanning electron microscopy (Zeiss Ultra 55 FESEM) equipped with an energy-dispersive X-ray analyzer (EDX) for elemental analysis.

2.4.2 Characterization of by-products of the electrolysis and other analytical measurements

The decrease of OG concentration and the analysis of the by-products were investigated using high performance liquid chromatography (HPLC) with a Hitachi Elite Lachrom chromatographic system equipped with a diode array detector. The chromatographic separations were performed on a Lichrospher 100RP-18C column (5 µm packing). The mobile phase was composed of methanol (eluent A) and an aqueous buffer solution NaH_2PO_4-Na_2HPO_4 with pH = 6.9 (eluent B). The flow rate was 1mL·min^{-1} at 298K and the injection volume was 80µL.

UV-Visible spectra were also obtained with A Hitachi Lachrom-Elite Chromatographic System equipped with diode array detector by changing the column for a tubular piece (without any packing inside). This allowed the sample to flow to the detector with low volume consumption.

The mineralization of the dye solutions was monitored from the decay of their chemical oxygen demand (COD). Total organic carbon (TOC) and total nitrogen (TN) COD was determined using a COD digester apparatus (Spectroquant® TR320) and a test analysis (Spectroquant® NOVA). The TOC and TN were determined with a Shimadzu TOC-VCSN analyzer based on the combustion-infrared method. The instrument operated at 720ºC and 20 µL sample injection with an air (free of CO_2) flow rate of 150 mL min^{-1}.

Fourier transform infrared spectroscopy (FTIR) was carried out at room temperature with a NICOLET 6700 FTIR spectrometer to determine the presence of functional groups in the extract. A ZnSe prism was used in the ATR device in which the bottom of the surface prism serves as the cavity for aqueous samples. The average spectra were obtained after 400 scans with a resolution of 6 cm^{-1} by subtracting the background signals obtained with an aqueous solution of 0.5 M Na_2SO_4.

Fluorescence emission spectra were recorded with a QuantaMasterTM 4 CW spectrofluorometer from Photon Technology International Inc (PTI®). The excitation wavelength was fixed at 340 nm and the emission spectra were recorded from 380 to 650 nm. A 75 W Xe light source and 1 cm quartz cells were used. Corrected emission spectra were obtained.

GC–MS analyses were performed using a Shimadzu GC–MSQP2010 gas chromatograph–mass spectrometer (GC-MS) equipped with a secondary electron multiplicator dinode (MSD). The column used was a Teknokroma S Meta X5, P/N TR-820232 capillary column (30 m × 0.25 mm × 0.25 μm). The solutions under study were treated as follows: 25 mL Orange G solutions were extracted with a total volume of 100 mL of dichloromethane for 3 times. The extracts were concentrated around 5 mL by rotary evaporator at 40 oC and then injected into the GC-MS. The following conditions were employed: gas (helium) flow rate of 22.6 mL min−1 and injection port temperature of 270 °C. GC temperature programme was as follows: 40 °C for 10 min, followed by a 12 °C min−1 ramp to 100 °C, then to 200 oC with 5 oC min-1, next a ramp to 270 oC with a 20 oC min-1 rate, finally 270 oC for 5 min [37,38]. Mass spectra were acquired in the electron impact mode. The m/z scan was from 35 to 500 and an ion source temperature of 200 °C.

2.4.3 Electrolysis of Orange G

To study the electrochemical behavior of the TC-RGO-Pt electrode for the oxidation and reduction processes of the Orange G molecule, a series of electrolysis of the OG solution were carried out in two different configurations of the electrochemical cell in the presence or absence of Cl- at the controlled potential. To study oxidation or reduction separately, a H-type (divided) cell is used using a cationic membrane type Nafion 117 to separate the cathodic and anodic compartments. The second configuration consists of an undivided double-walled electrochemical cell using three electrodes. In both electrolytic cells, the anode was a TC /RGO/Pt electrode. The cathode was either a Pt wire for the divided cell or a 1 cm^2 TC foil for

183 the undivided cell. The electrochemical monitoring is performed at a constant potential
184 provided by a Gamry 1000 potentiostat galvanostat at room temperature and constant stirring.
185 The counter-electrode potential was measured with a digital multimeter. Solutions containing
186 50 mg. dm^{-3} of Orange G at an initial pH of 6 were treated comparatively in divided and
187 undivided electrolytic cells. The initial pH was kept free (6.5 ± 0.5), without adjustment during
188 the process. The oxidation potential of the anode was kept to 1.1-1.4 V. The reduction potential
189 of the cathode was kept to -0.8 V and these potential values were chosen after previous
190 voltammetric studies (figures not shown). The mixture inside the cell is continuously stirred at
191 250 rpm using a magnetic stirrer. Samples of 1 mL are taken at regular intervals for HPLC
192 analysis. TOC, TN, COD, the average current efficiency (ACE) and the electrical energy
193 consumption per order (EEO) were combined to characterize the degradation performance.

194 The ACE related to the elimination of COD was based on the following equation [39]

195 $$ACE = \frac{COD_0 - COD_t}{8.I.t}.F.V.100 \qquad \text{Eq (1)}$$

196 Where COD_0 and COD_t are the initial values before treatment and at time t, respectively (g O_2
197 L^{-1}); F is the Faraday constant (96487 C mol^{-1}); V is the volume of the wastewater (L); I is the
198 applied current (A); t is the time of electrolysis (s); and 8 is the equivalent weight of oxygen.

199 One of the most important parameters affecting the performance of an electrochemical system
200 is the operating costs. With this purpose in mind, the electrical energy consumption per order
201 (EEO) was calculated in all cases. The calculus of EEO was chosen according to the report of
202 Bolton et al. [40]. This parameter is defined as the electrical energy in kilowatt-hour (kWh)
203 required to bring about a reduction by one order of magnitude in the concentration of the
204 contaminant by a unit of volume of contaminated water or air. The corresponding equation is
205 the following:

206 $$EEO = \frac{P \cdot t}{V \cdot \log\left(\frac{A_i}{A_f}\right)} \qquad \text{Eq (2)}$$

207 Where: P is the electric power (kW)(P=IV); t is the time of electrolysis (h); V is the volume
208 treated (m^3); A_i and A_f are the initial and final areas of the chromatographic peak associated
209 with the pollutant of interest.

3 Results and discussion

3.1 Electrode surface characterization

The coatings of TC-RGO-Pt were obtained using cyclic voltammetry with the procedure described in the electrode preparation section. The samples were examined using an FESEM technique and EDX analysis. Figures 2a and 2b show that the metallization of the electrode is homogeneous and retains its porosity. The Pt deposit has a granular appearance (Figure 2a inset) and consists of crystallites of different sizes on the surface of the fibers. The two successive deposits of RGO and Pt lead to the high rigidity of the material while keeping the essential properties of carbon fiber textile (lightness and microporosity). The electrode presented a uniform structure (see Figure 2b) which favors a longer life for the electrode and improves stability. To confirm the chemical composition of the TC/RGO /Pt substrate, EDX analysis was performed, as shown in Figure 2c. Pt and C are the major components of TC-RGO-Pt electrodes, and the presence of O is also observed. The results indicate that almost the entire surface was covered by Pt nanoparticles.

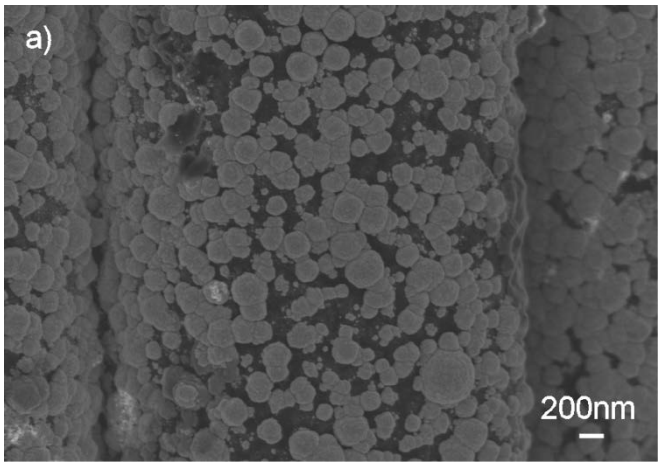

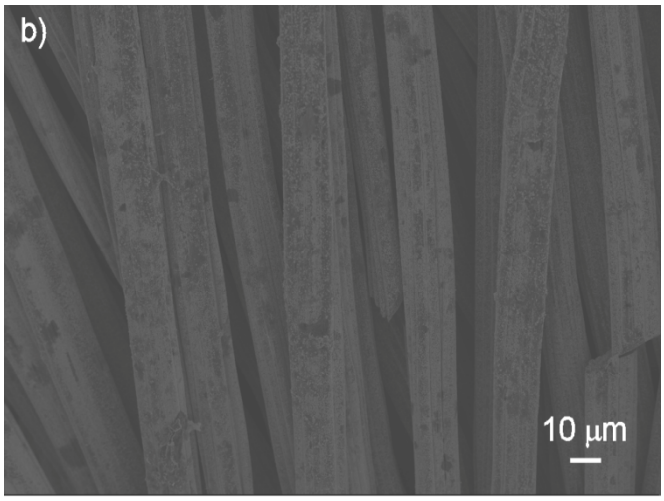

c)

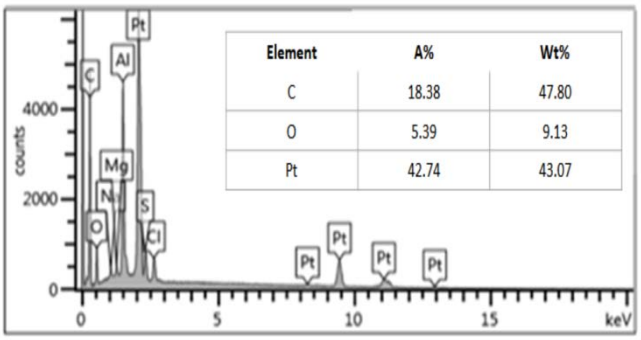

Fig. 2. a) and b) FESEM micrographs of TC–RGO–Pt electrode. c) EDX analysis

3.2 Characterization of the electrolytic treatment in the divided and undivided tank reactors

Effect of chloride addition:

The nature of the electrolyte significantly influences the efficiency of the anodic oxidation process. Adding an electrolyte to the solution improves the conductivity, accelerates the transfer of electrons, facilitates the flow of current, and therefore reduces the energy cost of the process. It is therefore interesting to study the effect of electrolytes on the degradation of organic compounds following electrolytic treatment [41]. To improve conductivity, Sodium sulfate is commonly used as the supporting electrolyte [42,43]. Chloride ions are used in some electrolytic treatments due to the strongly oxidizing properties of the active chlorine resulting from Cl electrolysis and which contributes to water disinfection [44-46]. In this study, sodium sulphate (0.1 M Na_2SO_4) in the presence and absence of chloride is used to study the influence of the supporting electrolyte on the degradation of Orange G. Our purpose is to study the possibility of enhancing the degradation rate by adding chloride to Na_2SO_4 electrolyte. Its influence on dye decolorization was checked by treating a 50 $mg.L^{-1}$ Orange G solution of initial pH=6.0 at the potentials of 1.1 V and 1.4V at 25 ◦C. Figs. 3a and 3b depict the change of Orange G dye removal efficiency for the electrolyzed solution in the divided and undivided tank reactor, respectively. Fig. 3a highlights that in the divided cell, the concentration of the pollutant decreases gradually with time to reach total removal after 21 h and 14 h of treatment in the absence and the presence of chloride, respectively. Degradation is slower in the absence of NaCl. In the reduction assays, degradation occurs, but is slower than in the oxidation cases. The rapid removal of the OG when adding $0.3g.L^{-1}$ NaCl to the 0.1M Na_2SO_4 as electrolyte can

be explained as follows the removal rates of the OG due to the higher oxidizing power of platinum materials, which favours the generation of hydroxyl radicals strongly adsorbed on the surface of the anode following the oxidation of water (equation 3) and are therefore not very mobile within the solution (chemisorption), the oxidation of organic molecules is therefore not very extensive and can present selectivity [47,48]. The presence or addition of chlorides to sulfates in a solution to be treated by electrochemical oxidation can accelerate the degradation process of organic matter. Indeed, organic matter can be oxidized at the electrode and also in situ of the solution by chemical reaction with active chlorine.

$$H_2O + M \rightarrow M(OH^{\cdot}) + e \qquad \text{Eq (3)}$$

$$M(OH^{\cdot}) \rightarrow MO + H^+ + e \qquad \text{Eq (4)}$$

These oxides can interact with organic pollutants (reaction 5) by oxidizing them and forming products of oxidized pollutants (products) [8].

$$MO + R \rightarrow M + products \qquad \text{Eq (5)}$$

Indeed, when NaCl is used, chloride ions can be oxidized to chlorine gas (Cl_2) at the anode (reaction 6), then react with water to form hypochlorous acid (HOCl) (equation 7) and thus add to the hydroxyl radicals for the destruction of organic pollution [49].

$$2Cl^- \rightarrow Cl_2 + 2é \qquad \text{Eq (6)}$$

$$Cl_2 + H_2O \rightarrow HClO + Cl^- + H^+ \qquad \text{Eq (7)}$$

The efficiency of Na_2SO_4 is because SO_4^{2-} ions can be oxidized at the anode to form persulphate ions (equation 8). Due to their high reactivity, the persulphate ions can react with organic compounds and thus increase the OG degradation rate [49].

$$2{SO_4}^{2-} \rightarrow {S_2O_8}^{2-} + 2é \qquad \text{Eq (8)}$$

$$HO^{\cdot} + {SO_4}^{2-} \rightarrow {SO_4}^{\cdot -} + HO^- \qquad \text{Eq (9)}$$

$${SO_4}^{\cdot -} + {SO_4}^{\cdot -} \rightarrow 2{S_2O_8}^{2-} \qquad \text{Eq (10)}$$

It is not recommended to use high concentrations of electrolyte due to possible formation of a layer of salt on the surface of the electrode, which reduces the number of radical hydroxyls formed and hinders the migration of organic matter to the surface of the electrode. These results are in agreement with those obtained by other researchers [50].

Moreover, it has been observed that in the undivided cell, the best percentage of removal is obtained with a total degradation of Orange G after only 5 h (Fig. 3b). In this case, a small addition of chloride is not necessary to obtain the best rate of removal (i.e. it improves the mineralization rate of the Orange G dye and decreases the necessary electrolysis time).

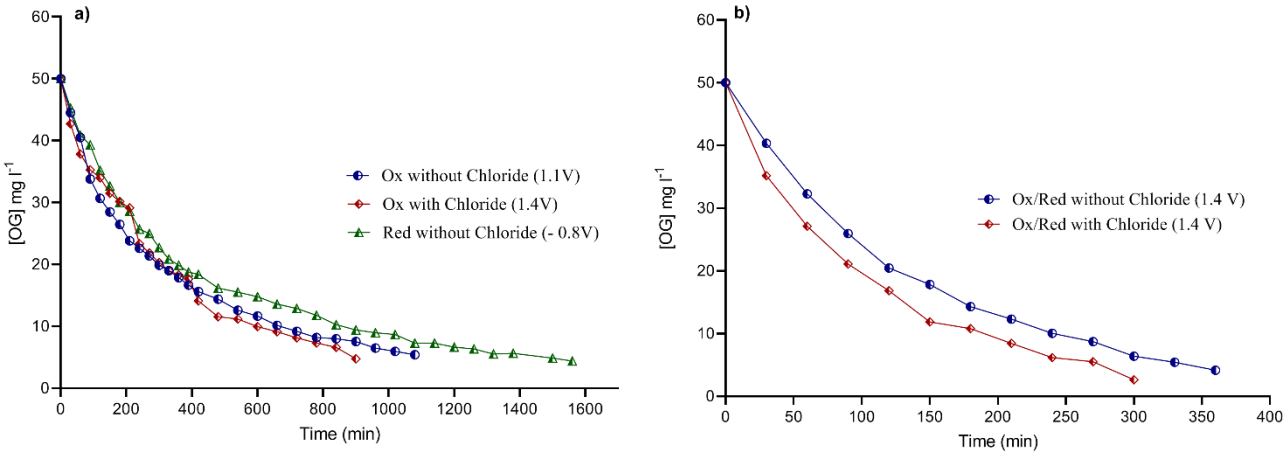

Fig. 3. Effect of supporting electrolyte on the decay of the dye during the electrolytic treatment of 50 ml of 50 mg.L^{-1} Orange G with or without chloride. (a) Divided TC-RGO-Pt/Pt tank reactor and (b) undivided TC-RGO-Pt/TC tank reactor.

3.3 Orange G degradation monitoring

HPLC technique was employed to evaluate the variation of dye concentration with electrolysis time and the generation of intermediates during the electrochemical processes. Fig 4 shows the evolution of the chromatographic profile during electrolysis. Chromatograms of treated solutions displayed a well-defined peak at a retention time (t_R) of 6.7 min for Orange G, allowing the analysis of its decay in the experiments performed in both cells. Significant removal of Orange G is observed for each cell used in the electrolytic treatment. However, the percentage of degradation of Orange G is different for the two configuration cells. As is shown in the chromatograms (Fig. 4). The initial peaks at a retention time of 6.7 min disappear during the electrolysis and there are some byproducts formed during anodic oxidation treatment. In both cells used, Orange G intermediate by-products appeared at different retention times.

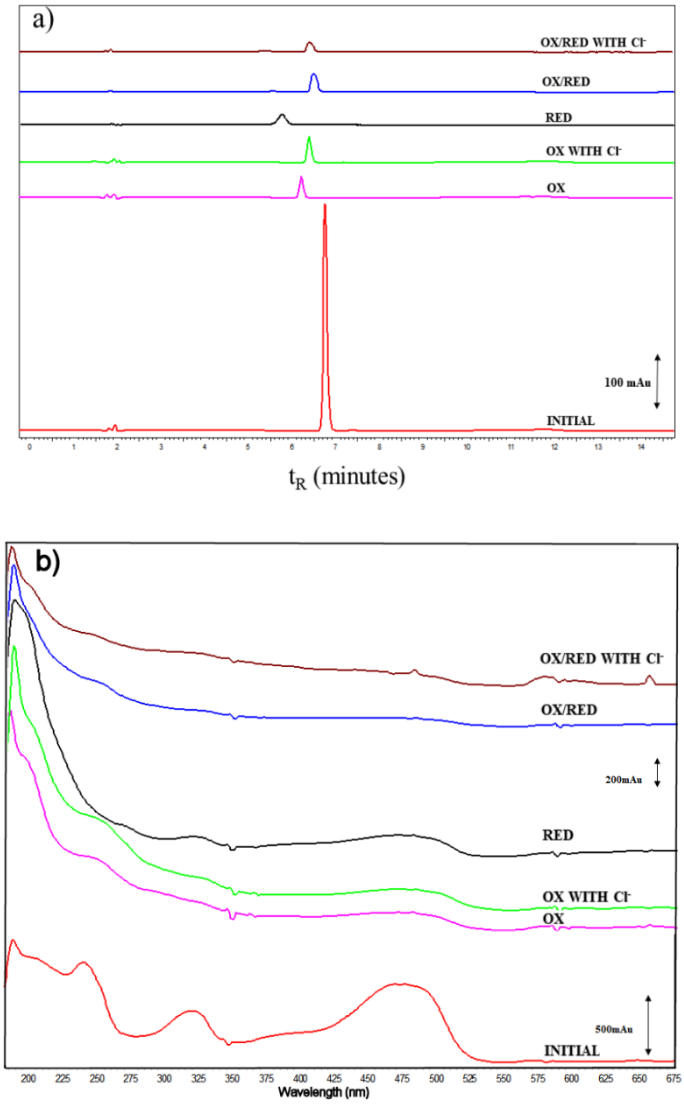

Fig. 4. a) HPLC chromatograms of the solutions before and after the different electrolysis. b) UV-Vis spectra of the solutions before and after the different electrolysis (notice that the scale of the initial spectrum is different from those after electrolysis).

HPLC results are confirmed by those obtained with the variation of COD, TOC, and TN removal. Fig. 5 shows the decrease in TOC, COD, and TN for both electrolytes and both cells at a similar loaded charge to that needed for total decolorization. The removal efficiency of the oxidation is higher in the presence of chloride and the use of undivided cells permit a higher mineralization in the absent of chloride.

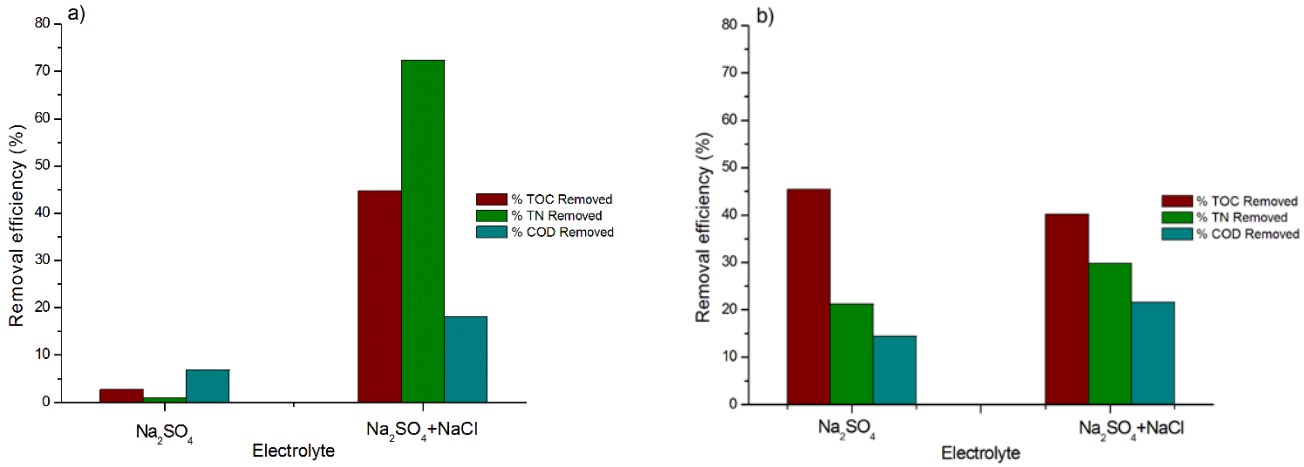

Fig. 5. Removal efficiency (%) of TOC, TN, and COD in the presence and absence of chloride as the electrolyte, after a loaded charge of around that needed for total decolorization: a) divided cell and b) undivided cell

3.4 Energy assessment: the average current efficiency (ACE) and the electrical energy consumption per order (EEO)

Electrical energy consumption and average current efficiency are very important economic parameters. Table 1 shows the variation of both parameters in both studied cells. EEO values are low and similar in all the studied cases. Nevertheless, this parameter decreases when chloride electrolytes or undivided cells are used. The differences are greater for ACE. These values substantially increase in the same way. It is noteworthy that a small concentration of chloride (0.3 g L^{-1}) is sufficient to promote important dye mineralization.

Table 1: The average current efficiency (ACE) and the electrical energy consumption per order (EEO) after electrolysis

CELL	POTENTIAL (V)	CHLORIDE	*Q* (Ah L^{-1})	DEGRADATION (%)	EEO (kWh m^{-3} $order^{-1}$)	ACE (%)
Divided	1.10	NO	0.31	90.00	0.344	16.18
	1.10	YES	0.24	92,34	0.236	38.34
	1.40	YES	0.17	92.07	0.219	75.88
	-0.80	NO	0.29	91.75	0.216	30.93
Undivided	1.4	NO	0.16	92.00	0.204	65.00
	1.4	YES	0.17	94.53	0.189	91.90

3.5 Product analysis of the solutions electrolyzed

The experimental UV-visible spectrum of Orange G (Figure 4b) before reaction consists of three main peaks at 250, 330, and 480 nm, plus a shoulder peak at between 380-420 nm [51,33]. The band at 480nm plus a shoulder peak at 421 nm are attributed respectively to the azo-bonds

of hydrozon [52] and the conjugated structure formed by the azo bond ($\pi \rightarrow \pi*$ transition related to the –N=N– group)[53]. The band centered at 330 nm derives from π–π* transition between π system of naphthalene ring, the SO_3 groups, and the π* system of the – N=N- azo [51]. The peak at 250 nm is assigned to benzene rings of OG. During the electrolysis, the bands at 330 nm and 480 nm gradually decrease until almost disappearing after treatment in both cells. This indicates the destruction of the chromophoric group and its conjugated bond. The strong decreases in the band at 330 nm indicate not only the destruction of the conjugated system of which the -N=N- bond is a part, but also of the naphthalene ring. The band around 250 nm decreases slowly but remains after electrolysis. This indicates that the aromatic rings were still present after the electrolysis [51].

The OG degradation and intermediate formation were also evidenced by the changes of FTIR spectra. Fig.6 shows the FTIR spectra before and after electrolysis. The spectra were obtained from 4000 to 400 cm^{-1}, but it is shown here only the range 1800-900 cm^{-1} where the effects of degradation are detectable.

In the FTIR spectrum of the solution used before electrolysis, a broad band between 1600 cm^{-1} and 1700 cm^{-1} (centered around 1650 cm^{-1}) can be observed; this band may be associated with the C-C stretching mode of the naphthalene ring, or the tautomeric form of chromophore group of the Orange G molecule (C = N $^{-}$) [54,55]. A second band centered at 1100 cm^{-1} can be observed that could be assigned to the presence of the C-OH band in the dye structure (C-O stretching vibration) [56]. This band remains in the FTIR spectra after all the electrochemical treatments.

The spectrum after the electrooxidation shows that the band at around 1625 cm^{-1} diminishes after the oxidation-reduction has completely disappeared which is an indication of the decolorization of the solution and naphthalene ring degradation.

After the reduction, the band at around 1625 cm^{-1} changes its shape and intensity and this is probably due to the appearance of an overlapped band associated with N-H (amines) deformation vibration. Moreover, two new bands centered at 1550 cm^{-1} and 1400 cm-1 appear. The first could be associated with N-H bending of imine (C = N – H). The band centered at 1400 cm^{-1} could be associated with α-naphthol (O-H deformation and C-O stretching vibration combination) [54].

Data from FTIR spectra provided the evidence to support that OG was attacked at several sites, including the sulfonyl group, C–N bond, and phenyl group, and other compounds like long-chain alkanes and compounds with carbonyl group were formed.

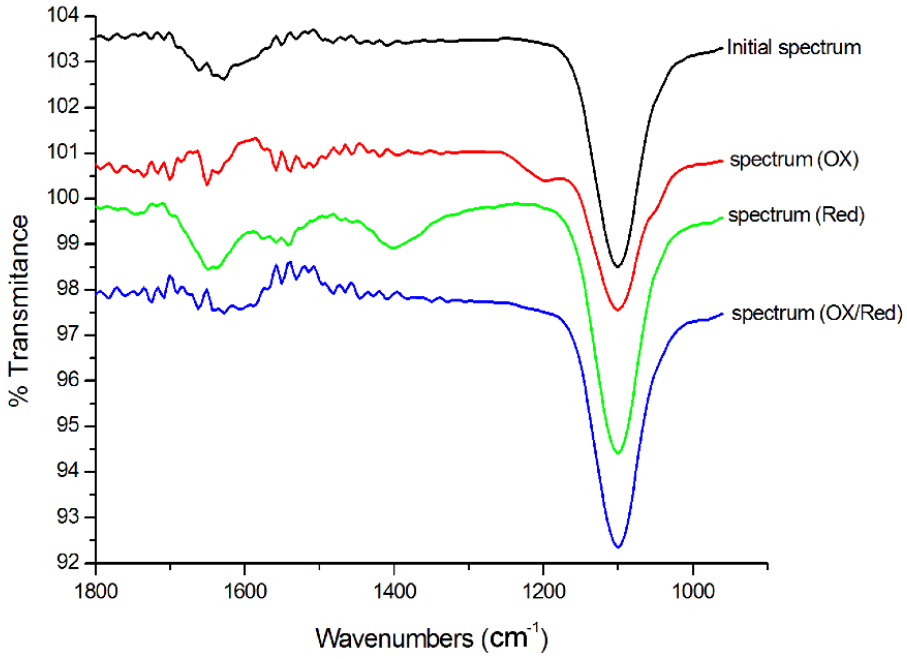

.

Fig. 6. FTIR spectra of the OG solution before and after electrolysis.

GC-MS analyses were carried out to identify some degradation by-products of Orange G solutions [37,38]. Fig.7a shows the GC chromatographs of Orange G solutions treated by electro-oxidation at 1.1 V with 0.1 M sodium sulfate. MS analyses showed the existence of the following by-products: cis-Aconitic anhydride, 5-Aminoisoxazole, 2-Ethyl-1-butanol, 3-Cyclohexen-1-ol, 1,3-Cyclohexanediol and Tetrahydro-4H-pyran-4-ol. Fig. 7b shows the GC chromatographs of Orange G solutions treated by electro-reduction at -0.8 V with 0.1 M sodium sulfate, MS analyses showed aniline as by-product. The GC chromatographs of samples treated by electro-oxidation at 1.1 V with 0.1 M sodium sulfate + 0.3 g/L sodium chloride is shown in Fig. 8c. MS analyses showed the existence of the followings by-products: cis-Aconitic anhydride, pyridine-1-oxide, acetaldol (3-Hydroxybutanal) and itaconic anhydride (dihydro-3-methylene-2,5-furandione).

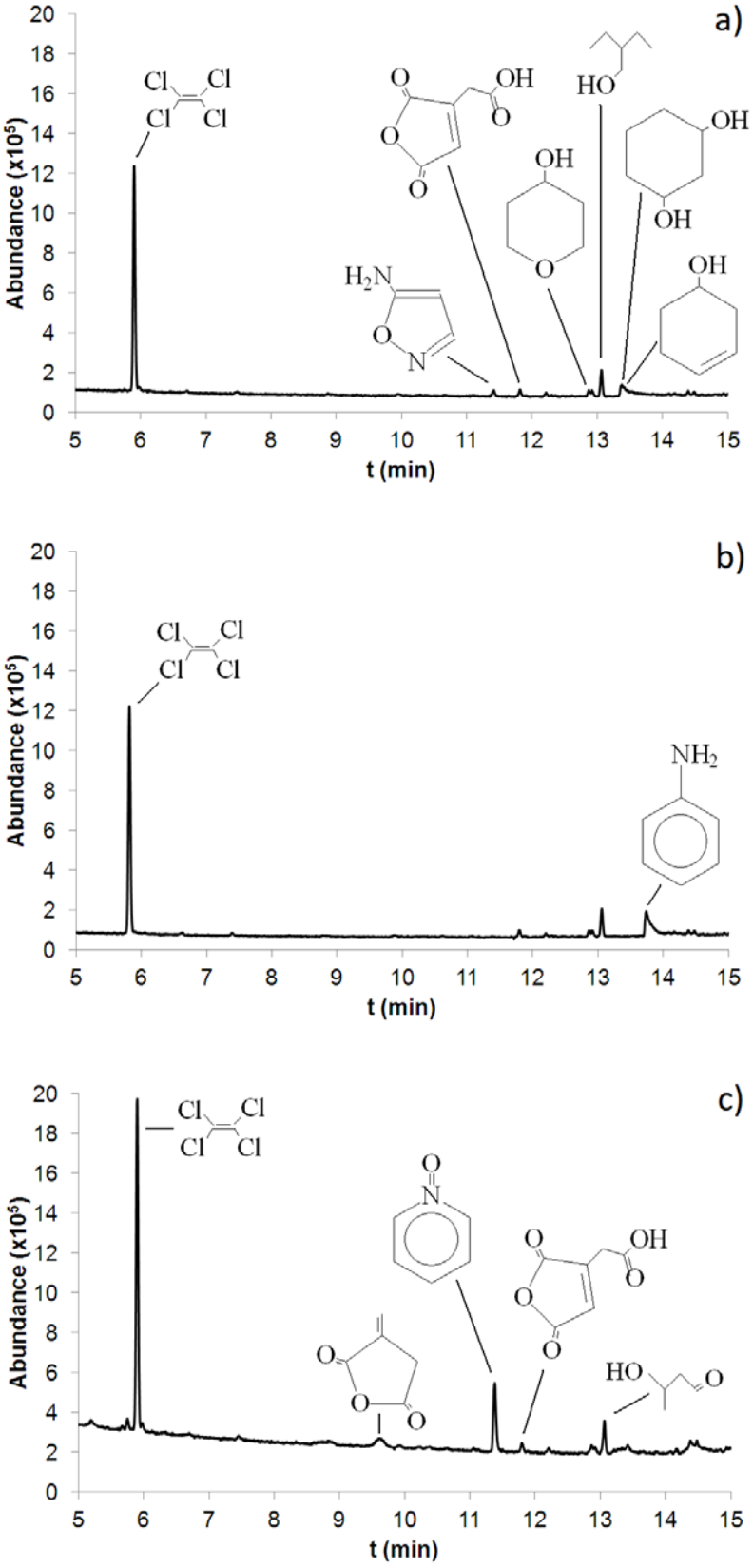

Fig. 7. GC chromatograms of Orange G solutions treated by: a) electro-oxidation at 1.1 V with 0.1 M sodium sulfate b) electro-reduction at -0.8 V with 0.1 M sodium sulfate c) electro-oxidation at 1.1 V

with 0.1 M sodium sulfate + 0.3 g/L sodium chloride. Chromatographs peaks are assigned by MS analyses.

3.6 Fluorescence analysis

A deeper study of the electrolysis was made and the fluorescence emission spectra of the initial and final samples are presented. Fig. 8 shows the fluorescence emission spectra for the Orange G initial sample and Orange G treated samples. Very low fluorescence emissions were obtained for the initial Orange G solution. Photoisomerisation, excimer, and exciplex formation almost totally ended the fluorescence in azo dyes [57]. The break of the azo bond (-N=N-) provides a high fluorescence emission due to the aromatic compounds in the solution; either benzene and naphthalene compounds. All Orange G samples after electrolysis showed a significant increase in fluorescence emission. The emission was considerably higher in divided electrochemical cells (oxidation) with chlorides at 1.1 V. The fluorescence emission in divided cells (oxidation) with chlorides at 1.4 V, and also the reduction (a little less) without chlorides at -0.8 V, had fairly high fluorescence values concerning the other electrolyses.

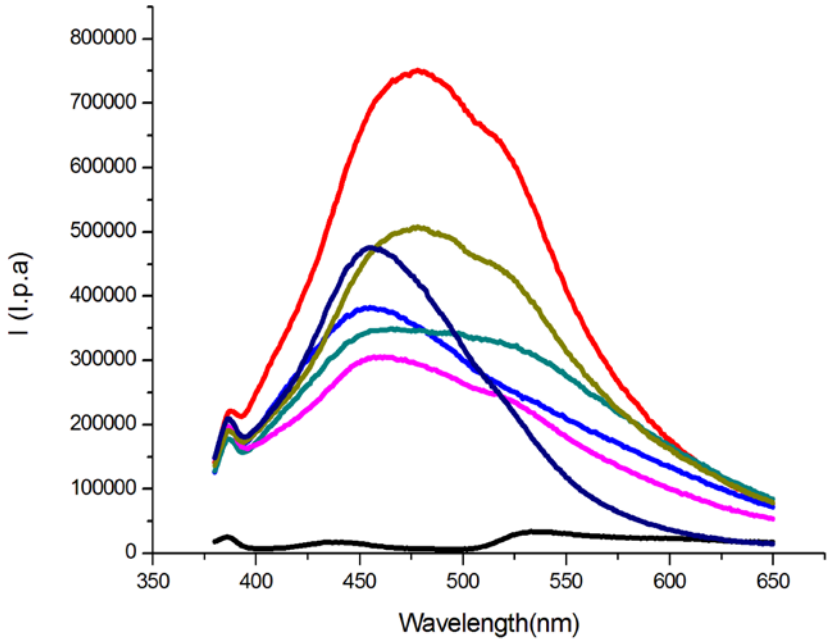

Fig. 8. Fluorescence emission spectra of Orange G solution for: — Initial sample; — After oxidation in the divided cell with Cl^- at 1.1 V; — After oxidation in a divided cell with Cl^- at 1.4 V; — After the reduction in a divided cell without Cl^- at -0.8 V; — After oxidation-reduction in an undivided cell without Cl^- at 1.4 V; — After oxidation-reduction in an undivided cell with Cl^- at 1.4 V; — After oxidation in a divided cell without Cl^- at 1.1 V.

Oxidation electrolysis in divided cells with chlorides at 1.1 V provided a greater amount of benzene and naphthalene compounds, as by-products of the degradation of the Orange G samples.

From the spectroscopic results shown above, a reaction mechanism such as the one shown in Fig 9 could be proposed.

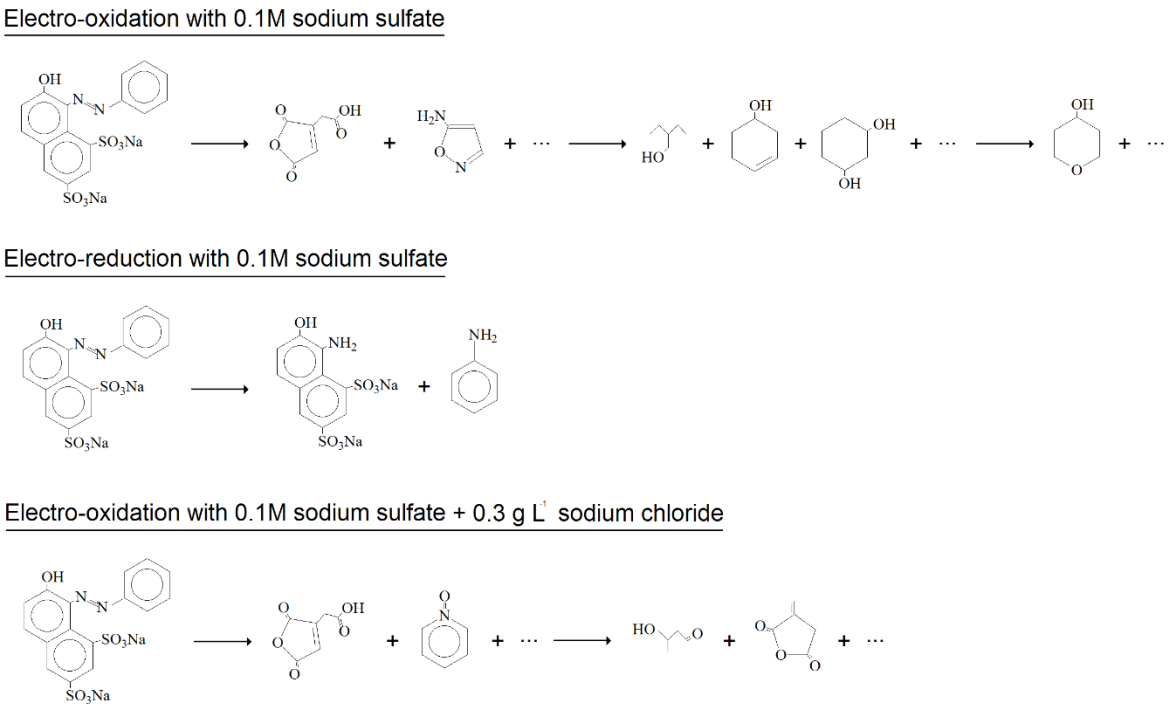

Fig. 9. Oxidation and reduction reaction mechanisms.

3.7 Electrode stability

The FESEM images of the TC-RGO-Pt electrode used as an anode after oxidation of OG at 1.1 V in absence of chloride, and 1.1 V and 1.4V in the presence of chloride, are shown in Figures 10a, 10b, and 10c, respectively. It is observed that the dispersed Pt is still present on the surface of the RGO, although a small reduction in the number of active sites on the surface was detected after electrolysis, which could not represent a significant influence on reversibility and electrocatalytic properties. The EDX results reveal a decrease of 11%, 32%, and 46% in the amounts of Pt after electrolysis at 1.1 V in absence of chloride, and 1.1 V, and 1.4 V in the presence of chloride, respectively. Therefore, the presence of chloride and the increase in the potential decrease the overall amount of Pt; but the degradation of the surface of the electrode is slight.

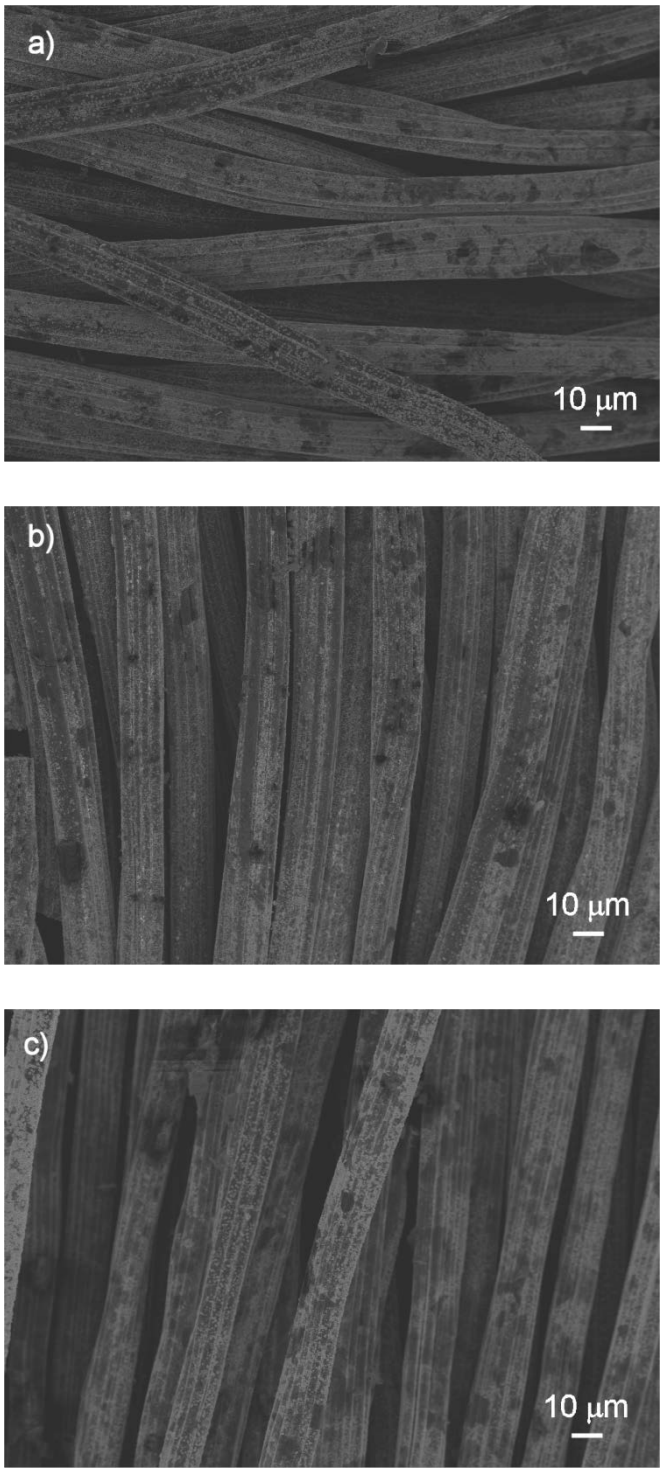

Fig. 10. FESEM micrographs of TC–RGO–Pt electrode after electrolysis: a) oxidation at 1.1 V without chloride; b) oxidation at 1.1 V with chloride; c) oxidation at 1.4 V with chloride

4 Conclusion

Carbon textile electrodes were successfully modified with RGO and Pt nanoparticles by CV. The electrodes obtained were characterized by field emission scanning electron microscopy

(FESEM) and EDX analysis. The analyses by FESEM confirmed that the textile surface was covered by Pt nanoparticles. Electrolysis of Orange G solutions was carried out using these modified materials as electrodes. It was also found that the degree of elimination is highly influenced by the cell configuration. Based on the described results we can conclude that the Orange G dye removal process was always faster in the undivided cell where anodic and cathodic compartments are not separated. Similarly, its TOC, COD, and TN were much more efficiently removed in this system where the degradation was achieved in less than 0.17 Ah L^{-1} in the presence of chloride ions. In such conditions, better current efficiency was obtained, as well as lower energy consumption (0.189 kWh m^{-3} $order^{-1}$). Although spectroscopic results indicate the destruction of the chromophoric group and its conjugated bond and the naphthalene ring. The aromatic rings were present in the solution and not entirely eliminated.

These results support the viability of this type of electrode and show its mechanical properties, which enable obtaining electrodes with a large flexibility, dimensional versatility, and a high specific area, which should make it possible to design more compact electrochemical cells. It must also be demonstrated that these properties can be improved by increasing their stability, conductivity, specific surface, and electroactivity by surface modifications. And finally, they are useful both as anodes and cathodes with high efficiency and low energy consumption in the electrolysis – all at a competitive price.

Acknowledgements

The authors wish to thank the Spanish Agencia Estatal de Investigación (AEI) and European Union (FEDER funds) for the financial support (contract MAT2016-77742-C2-1-P) and Chemviron Carbon who kindly donated the FlexzorbTM FM10 activated carbon fabrics. The invitation by the E3TECH Spanish Network of Excellence (CTQ2017-90659-REDT (MEIC/AEI)) is kindly acknowledged.

References

[1] J. Wang, T. Zhang, Y. Mei, B. Pan, Treatment of reverse-osmosis concentrate of printing and dyeing wastewater by electro-oxidation process with controlled oxidation-reduction potential (ORP), Chemosphere. 201 (2018) 621–626. https://doi.org/10.1016/j.chemosphere.2018.03.051.

[2] R.A. Damodar, K. Jagannathan, T. Swaminathan, Decolourization of reactive dyes by thin film immobilized surface photoreactor using solar irradiation, Sol. Energy. 81 (2007) 1–7. https://doi.org/10.1016/j.solener.2006.07.001.

[3] R.E. Palma-Goyes, J. Silva-Agredo, I. González, R.A. Torres-Palma, Comparative degradation of indigo carmine by electrochemical oxidation and advanced oxidation processes, Electrochimica Acta. 140 (2014) 427–433. https://doi.org/10.1016/j.electacta.2014.06.096.

[4] S.L. Orozco, E.R. Bandala, C.A. Arancibia-Bulnes, B. Serrano, R. Suárez-Parra, I. Hernández-Pérez, Effect of iron salt on the color removal of water containing the azo-dye reactive blue 69 using photo-assisted Fe (II)/H2O2 and Fe (III)/H2O2 systems, J. Photochem. Photobiol. Chem. 198 (2008) 144–149.

[5] F.C. Moreira, R.A.R. Boaventura, E. Brillas, V.J.P. Vilar, Electrochemical advanced oxidation processes: A review on their application to synthetic and real wastewaters, Appl. Catal. B Environ. 202 (2017) 217–261. https://doi.org/10.1016/j.apcatb.2016.08.037.

[6] Y. Samet, L. Agengui, R. Abdelhédi, Anodic oxidation of chlorpyrifos in aqueous solution at lead dioxide electrodes, J. Electroanal. Chem. 650 (2010) 152–158.

[7] M.A. Tarr, Chemical degradation methods for wastes and pollutants: environmental and industrial applications, CRC press, 2003.

[8] C.A. Martinez-Huitle, S. Ferro, Electrochemical oxidation of organic pollutants for the wastewater treatment: direct and indirect processes, Chem. Soc. Rev. 35 (2006) 1324–1340.

[9] M. Zhou, H. Särkkä, M. Sillanpää, A comparative experimental study on methyl orange degradation by electrochemical oxidation on BDD and MMO electrodes, Sep. Purif. Technol. 78 (2011) 290–297.

[10] F. Yi, S. Chen, Effect of activated carbon fiber anode structure and electrolysis conditions on electrochemical degradation of dye wastewater, J. Hazard. Mater. 157 (2008) 79–87.

[11] A.G. Vlyssides, M. Loizidou, P.K. Karlis, A.A. Zorpas, D. Papaioannou, Electrochemical oxidation of a textile dye wastewater using a Pt/Ti electrode, J. Hazard. Mater. 70 (1999) 41–52.

[12] L. Xu, M. Li, W. Xu, Preparation and characterization of Ti/SnO2-Sb electrode with copper nanorods for AR 73 removal, Electrochimica Acta. 166 (2015) 64–72.

[13] V.M. Vasconcelos, C. Ponce-de-León, J.L. Nava, M.R. Lanza, Electrochemical degradation of RB-5 dye by anodic oxidation, electro-Fenton and by combining anodic

488 oxidation–electro-Fenton in a filter-press flow cell, J. Electroanal. Chem. 765 (2016) 179–
489 187.
490 [14] M. Panizza, A. Barbucci, R. Ricotti, G. Cerisola, Electrochemical degradation of
491 methylene blue, Sep. Purif. Technol. 54 (2007) 382–387.
492 [15] M. Muthukumar, M.T. Karuppiah, G.B. Raju, Electrochemical removal of CI Acid orange
493 10 from aqueous solutions, Sep. Purif. Technol. 55 (2007) 198–205.
494 [16] W.-L. Chou, C.-T. Wang, C.-P. Chang, M.-H. Chung, Y.-M. Kuo, Removal of color and
495 COD from dyeing wastewater by paired electrochemical oxidation, Fresenius Environ.
496 Bull. 20 (2011) 78–85.
497 [17] F.J. Recio, P. Herrasti, I. Sirés, A.N. Kulak, D.V. Bavykin, C. Ponce-de-León, F.C. Walsh,
498 The preparation of PbO2 coatings on reticulated vitreous carbon for the electro-oxidation
499 of organic pollutants, Electrochimica Acta. 56 (2011) 5158–5165.
500 [18] I. Yahiaoui, F. Aissani-Benissad, F. Fourcade, A. Amrane, Response surface methodology
501 for the optimization of the electrochemical degradation of phenol on Pb/PbO2 electrode,
502 Environ. Prog. Sustain. Energy. 31 (2012) 515–523.
503 [19] I. Yahiaoui, F. Aissani-Benissad, F. Fourcade, A. Amrane, Removal of tetracycline
504 hydrochloride from water based on direct anodic oxidation (Pb/PbO2 electrode) coupled
505 to activated sludge culture, Chem. Eng. J. 221 (2013) 418–425.
506 [20] L. Xu, Z. Guo, L. Du, Anodic oxidation of azo dye CI Acid Red 73 by the yttrium-doped
507 Ti/SnO 2-Sb electrodes, Front. Chem. Sci. Eng. 7 (2013) 338–346.
508 [21] Á. Anglada, A. Urtiaga, I. Ortiz, Contributions of electrochemical oxidation to waste-
509 water treatment: fundamentals and review of applications, J. Chem. Technol. Biotechnol.
510 84 (2009) 1747–1755. https://doi.org/10.1002/jctb.2214.
511 [22] Y. Samet, S.C. Elaoud, S. Ammar, R. Abdelhedi, Electrochemical degradation of 4-
512 chloroguaiacol for wastewater treatment using PbO2 anodes, J. Hazard. Mater. 138 (2006)
513 614–619. https://doi.org/10.1016/j.jhazmat.2006.05.100.
514 [23] J.M. Aquino, R.C. Rocha-Filho, L.A.M. Ruotolo, N. Bocchi, S.R. Biaggio,
515 Electrochemical degradation of a real textile wastewater using β-PbO2 and DSA® anodes,
516 Chem. Eng. J. 251 (2014) 138–145. https://doi.org/10.1016/j.cej.2014.04.032.
517 [24] L. Fan, Y. Zhou, W. Yang, G. Chen, F. Yang, Electrochemical degradation of aqueous
518 solution of Amaranth azo dye on ACF under potentiostatic model, Dyes Pigments. 76
519 (2008) 440–446.
520 [25] Y. Liu, Application of graphene oxide in water treatment, IOP Conf. Ser. Earth Environ.
521 Sci. 94 (2017) 012060. https://doi.org/10.1088/1755-1315/94/1/012060.

[26] G.M. Scheuermann, L. Rumi, P. Steurer, W. Bannwarth, R. Mülhaupt, Palladium Nanoparticles on Graphite Oxide and Its Functionalized Graphene Derivatives as Highly Active Catalysts for the Suzuki−Miyaura Coupling Reaction, J. Am. Chem. Soc. 131 (2009) 8262–8270. https://doi.org/10.1021/ja901105a.

[27] S. Park, R.S. Ruoff, Chemical methods for the production of graphenes, Nat. Nanotechnol. 4 (2009) 217–224.

[28] T. Zhou, F. Chen, C. Tang, H. Bai, Q. Zhang, H. Deng, Q. Fu, The preparation of high performance and conductive poly (vinyl alcohol)/graphene nanocomposite via reducing graphite oxide with sodium hydrosulfite, Compos. Sci. Technol. 71 (2011) 1266–1270.

[29] L. Chen, Y. Tang, K. Wang, C. Liu, S. Luo, Direct electrodeposition of reduced graphene oxide on glassy carbon electrode and its electrochemical application, Electrochem. Commun. 13 (2011) 133–137.

[30] S.-X. Guo, S.-F. Zhao, A.M. Bond, J. Zhang, Simplifying the evaluation of graphene modified electrode performance using rotating disk electrode voltammetry, Langmuir. 28 (2012) 5275–5285.

[31] C. Xu, X. Wang, J. Zhu, Graphene- metal particle nanocomposites, J. Phys. Chem. C. 112 (2008) 19841–19845.

[32] R. Nie, J. Wang, L. Wang, Y. Qin, P. Chen, Z. Hou, Platinum supported on reduced graphene oxide as a catalyst for hydrogenation of nitroarenes, Carbon. 50 (2012) 586–596.

[33] H. Hamous, A. Khenifi, Z. Bouberka, Z. Derriche, H. Hamous, A. Khenifi, Z. Bouberka, Z. Derriche, Electrochemical degradation of Orange G in K 2 SO 4 and KCl medium, Environ. Eng. Res. 25 (2019) 571–578.

[34] A. El-Ghenymy, F. Centellas, J.A. Garrido, R.M. Rodríguez, I. Sirés, P.L. Cabot, E. Brillas, Decolorization and mineralization of Orange G azo dye solutions by anodic oxidation with a boron-doped diamond anode in divided and undivided tank reactors, Electrochimica Acta. 130 (2014) 568–576.

[35] T.-F. Wu, W.-C. Lin, Y.-C. Hsiao, C.-H. Su, C.-C. Hu, C.-P. Huang, R. Muniyandi, Electrochemical Photocatalytic Degradation of Orange G Using TiO_2 Films Prepared by Cathodic Deposition, J. Electrochem. Soc. 161 (2014) H762–H769. https://doi.org/10.1149/2.0521412jes.

[36] H. Chenini, K. Djebbar, S.M. Zendaoui, T. Sehili, B. Zouchoune, Removal of an Azo Dye (Orange G) By Various Methods in Homogenious Phase. Comparative Study, in: 1975.

555 [37] S. Rodriguez, L. Vasquez, D. Costa, A. Romero, A. Santos, Oxidation of Orange G by
556 persulfate activated by Fe (II), Fe (III) and zero valent iron (ZVI), Chemosphere 101 (2014)
557 86–92.

558 [38] X. Zhong, S. Royer, H. Zhang, Q. Huang, L. Xiang, S. Valange, Joel Barrault, Mesoporous
559 silica iron-doped as stable and efficient heterogeneous catalyst for the degradation of CI
560 Acid Orange 7 using sono–photo-Fenton process, Separation and Purification Technology
561 80 (2011) 163–171.

562 [39] M. Panizza, G. Cerisola, Removal of colour and COD from wastewater containing acid
563 blue 22 by electrochemical oxidation, J. Hazard. Mater. 153 (2008) 83–88.
564 [40] J.R. Bolton, K.G. Bircher, W. Tumas, C.A. Tolman, Figures-of-merit for the technical
565 development and application of advanced oxidation technologies for both electric-and
566 solar-driven systems (IUPAC Technical Report), Pure Appl. Chem. 73 (2001) 627–637.
567 [41] V. Khandegar, A.K. Saroha, Electrocoagulation for the treatment of textile industry
568 effluent – A review, J. Environ. Manage. 128 (2013) 949–963.
569 https://doi.org/10.1016/j.jenvman.2013.06.043.
570 [42] E. Isarain-Chávez, M.D. Baró, E. Rossinyol, U. Morales-Ortiz, J. Sort, E. Brillas, E.
571 Pellicer, Comparative electrochemical oxidation of methyl orange azo dye using Ti/Ir-Pb,
572 Ti/Ir-Sn, Ti/Ru-Pb, Ti/Pt-Pd and Ti/RuO2 anodes, Electrochimica Acta. 244 (2017) 199–
573 208.
574 [43] P.V. Nidheesh, R. Gandhimathi, Trends in electro-Fenton process for water and
575 wastewater treatment: an overview, Desalination. 299 (2012) 1–15.
576 [44] I. Sirés, E. Brillas, M.A. Oturan, M.A. Rodrigo, M. Panizza, Electrochemical advanced
577 oxidation processes: today and tomorrow. A review, Environ. Sci. Pollut. Res. 21 (2014)
578 8336–8367. https://doi.org/10.1007/s11356-014-2783-1.
579 [45] C. Comninellis, G. Chen, eds., Electrochemistry for the Environment, Springer New York,
580 New York, NY, 2010. https://doi.org/10.1007/978-0-387-68318-8.
581 [46] M. Panizza, G. Cerisola, Direct And Mediated Anodic Oxidation of Organic Pollutants,
582 Chem. Rev. 109 (2009) 6541–6569. https://doi.org/10.1021/cr9001319.
583 [47] M. Panizza, G. Cerisola, Influence of anode material on the electrochemical oxidation of
584 2-naphthol: Part 2. Bulk electrolysis experiments, Electrochimica Acta. 49 (2004) 3221–
585 3226.

[48] E. Brillas, I. Sirés, C. Arias, P.L. Cabot, F. Centellas, R.M. Rodríguez, J.A. Garrido, Mineralization of paracetamol in aqueous medium by anodic oxidation with a boron-doped diamond electrode, Chemosphere. 58 (2005) 399–406.

[49] F.C. Moreira, R.A.R. Boaventura, E. Brillas, V.J.P. Vilar, Electrochemical advanced oxidation processes: A review on their application to synthetic and real wastewaters, Appl. Catal. B Environ. 202 (2017) 217–261. https://doi.org/10.1016/j.apcatb.2016.08.037.

[50] L. Chachou, Y. Gueraini, Y. Bouhalouane, S. Poncin, H.Z. Li, K. Bensadok, Application of the electro-Fenton process for cutting fluid mineralization, Environ. Technol. 36 (2015) 1924–1932. https://doi.org/10.1080/09593330.2015.1016120.

[51] X.-R. Xu, X.-Z. Li, Degradation of azo dye Orange G in aqueous solutions by persulfate with ferrous ion, Sep. Purif. Technol. 72 (2010) 105–111.

[52] C. Bauer, P. Jacques, A. Kalt, Photooxidation of an azo dye induced by visible light incident on the surface of TiO2, J. Photochem. Photobiol. Chem. 140 (2001) 87–92. https://doi.org/10.1016/S1010-6030(01)00391-4.

[53] H. Chenini, K. Djebbar, S.M. Zendaoui, Removal of an Azo Dye (Orange G) by Various Methods in Homogenious Phase: Comparative Study, Jordan J. Chem. 146 (2011) 1–13.

[54] G. Socrates, Infrared and Raman characteristic group frequencies: tables and charts, John Wiley & Sons, 2004.

[55] M. Snehalatha, C. Ravikumar, N. Sekar, V.S. Jayakumar, I.H. Joe, FT-Raman, IR and UV-visible spectral investigations and ab initio computations of a nonlinear food dye amaranth, J. Raman Spectrosc. Int. J. Orig. Work Asp. Raman Spectrosc. High. Order Process. Also Brillouin Rayleigh Scatt. 39 (2008) 928–936.

[56] P.A. Carneiro, C.S. Fugivara, R.F. Nogueira, N. Boralle, M.V. Zanon, A comparative study on chemical and electrochemical degradation of reactive blue 4 dye, Port. Electrochimica Acta. 21 (2003) 49–67.

[57] U. Warde, N. Sekar, NLOphoric mono-azo dyes with negative solvatochromism and in-built ESIPT unit from ethyl 1, 3-dihydroxy-2-naphthoate: Estimation of excited state dipole moment and pH study, Dyes Pigments. 137 (2017) 384–394.